Carrier Dynamics in Si Nanowires Fabricated by Metal-Assisted Chemical Etching

Hao Tang,[†,∥] Li-Guo Zhu,[‡,§,⊥,∥] Liang Zhao,[‡] Xuejin Zhang,[†] Jie Shan,[‡,*] and Shuit-Tong Lee[¶,*]

[†]Center of Super-Diamond and Advanced Films (COSDAF) and Department of Physics and Materials Science, City University of Hong Kong, Hong Kong SAR, China, [‡]Department of Physics, Case Western Reserve University, 10900 Euclid Avenue, Cleveland, Ohio 44106, United States, [§]Department of Engineering Physics, Tsinghua University, Beijing 100084, China, [⊥]Institute of Fluid Physics, China Academy of Engineering Physics, Mianyang, Sichuan 621900, China, and [¶]Institute of Functional Nano & Soft Materials (FUNSOM), Soochow University, Suzhou, Jiangsu 215123, China. [∥]These authors contributed equally to this work.

ABSTRACT Silicon nanowire arrays fabricated by metal-assisted wet chemical etching have emerged as a promising architecture for solar energy harvesting applications. Here we investigate the dynamics and transport properties of photoexcited carriers in nanowires derived from an intrinsic silicon wafer using the terahertz (THz) time-domain spectroscopy. Both the dynamics and the pump fluence dependence of the photoinduced complex conductivity spectra up to several THz were measured. The photoinduced conductivity spectra follow a Lorentz dependence, arising from surface plasmon resonances in nanowires. The carrier lifetime was observed to approach 0.7 ns, which is limited primarily by surface trapping. The intrinsic carrier mobility was found to be ~1000 $cm^2/(V \cdot s)$. Compared to other silicon nanostructures, these relative high values observed for both the carrier lifetime and mobility are the consequences of high crystallinity and surface quality of the nanowires fabricated by the metal-assisted wet chemical etching method.

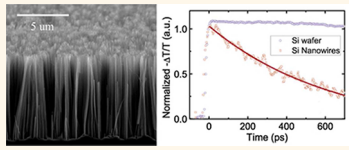

KEYWORDS: silicon nanowire · terahertz time-domain spectroscopy · surface band bending

Solar cells based on silicon micro- and nanowire arrays[1−8] are an attractive alternative to planar Si devices. They possess excellent light-harvesting capabilities through light scattering and trapping[9,10] and enhanced collection efficiencies of photogenerated charge carriers through short transport distances.[11] The structure is also advantageous for the fabrication of organic-Si nanowire heterojunctions. A conversion efficiency as high as 9.7% has been demonstrated in organic-Si nanowire heterojunctions.[1] Large-area arrays of Si nanowires can be grown on silicon wafers or flexible metal foils using the vapor−liquid−solid (VLS) process.[5−9] However, the use of metal catalysts, such as gold, results in increased carrier recombination within the wires, as well as significant surface recombination.[11,12] Metal-assisted wet chemical etching is an alternative method that can simply and cost-effectively fabricate silicon nanowire arrays from bulk Si at room temperature.[1−4,13] In this method, the doping density in nanowires can be controlled by that in the bulk Si wafers without introducing additional metal contaminations. The carrier lifetime and, consequently, the collection efficiency are expected to increase significantly.

Photoconductivity of chemically etched nanowires has been widely studied,[14] but direct information on its dynamics, particularly in the picosecond to nanosecond regime, crucial for understanding the charge separation and transport processes, is still not available. Scanning photocurrent microscopy has been employed to determine the carrier diffusion length in single-nanowire solar cells.[15] The carrier lifetime can be estimated if diffusion is dominated by bulk recombination. The technique, however, cannot differentiate bulk recombination from surface recombination. Furthermore, the surface band bending in etched silicon nanowires resulted from H-defect dangling bonds and H_2O and CO_2 adsorbates,[16,17] and its influence on charge separation[18] has been discussed. The direct effect of band bending on carrier mobility and lifetime in Si nanowires, however, remains unclear.

In this work, we apply the optical pump-terahertz (THz) probe spectroscopy to investigate the lifetime and transport properties of photogenerated carriers in chemically etched silicon nanowires. THz time-domain spectroscopy, based on the generation and detection of ultrafast electromagnetic transients, measures the frequency-dependent complex conductivity in a broad spectral range up to a few THz. With the addition of a pump optical pulse, the method allows probing of the ultrafast temporal evolution of transport

* Address correspondence to jie.shan@case.edu, apannale@suda.edu.cn.

Received for review April 30, 2012 and accepted August 14, 2012.

Published online August 15, 2012
10.1021/nn301891s

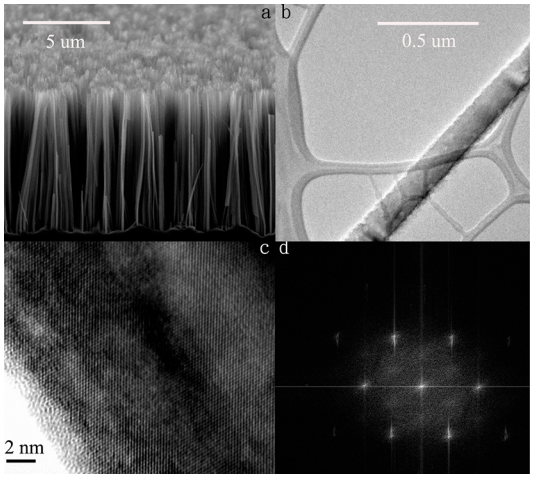

Figure 1. (a) SEM, (b) TEM, (c) high-resolution TEM images with (d) selected area electron diffraction pattern of silicon nanowires.

parameters with a picosecond to subpicosecond time resolution. The technique has been applied to the study of a variety of bulk and nanomaterials[19] including silicon nanocrystals,[20] CdSe nanocrystals,[21] TiO_2 nanotubes,[22] GaAs,[23] and Ge nanowires.[24] Our findings show that, in contrast to other Si nanostructures,[20,25] the photoinjected electrons in our chemically etched Si nanowires possess a relatively long lifetime of 0.7 ns and mobilities exceeding 1000 $cm^2/(V \cdot s)$. The long carrier lifetime and high mobility are consequences of high-quality crystallinity and surface properties of our samples.

RESULTS AND DISCUSSION

Silicon nanowire arrays were prepared on intrinsic (100) silicon wafers (Cemat Silicon S.A.; ≥20 000 Ωcm) *via* a Ag-assisted electroless chemical etching method.[13] Figure 1a shows the scanning electron microscopy (SEM) image of the as-grown silicon nanowire arrays, and Figure 1b is the transmission electron microscopy (TEM) image of a typical single nanowire. The wires are about 200−350 nm in diameter and several tens of micrometers in length. The high-resolution transmission electron microscopy (HRTEM) image (Figure 1c) and the selected area electron diffraction pattern (Figure 1d) clearly demonstrate that nanowires fabricated by chemical etching maintain the high-quality single-crystalline structure of the original silicon wafer.

For optical measurements, Si nanowires were transferred from the Si wafer to a quartz substrate, which is transparent in the THz regime. The nanowires were randomly distributed with an average areal density of about 0.15 nanowires per μm^2, corresponding to an areal filling fraction of 3 ± 1%. The intrinsic silicon (100) wafer was also measured for comparison. A typical optical pump/THz probe setup based on a Ti:sapphire amplifier centered at 800 nm with a repetition rate of 1 kHz and a pulse duration of 50 fs was employed.[19]

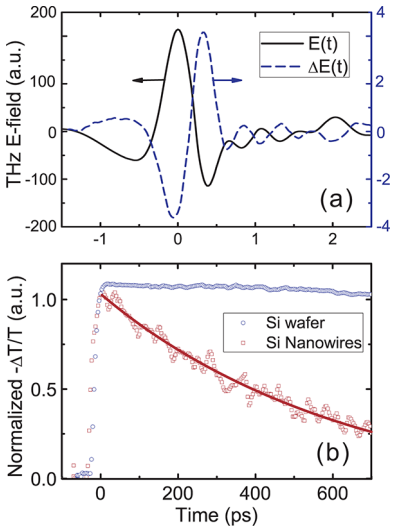

Figure 2. (a) Electric-field waveform of the THz radiation transmitted through unexcited samples $E(t)$ (black solid curve) and its photoinduced change $\Delta E(t)$ (blue dashed curve). (b) Pump-induced change in the peak (t_0) of the transmitted THz waveform, $\Delta E(t_0,\tau)$, for different pump−probe delay times τ, for Si nanowires (brown square), and the original Si wafer (blue circle). Solid curve is an exponential fit. Zero delay time is defined as the overlap of the pump optical pulse and the peak of the THz pulse transmitted through the sample. Note the carrier lifetime in bulk Si is known to be approximately microseconds. The reduction of the signal here arises from a minor imperfection of the overlap of the pump and probe beam at long delay times. The measurements on Si nanowires have been corrected based on the bulk result.

In brief, THz electromagnetic transients were generated and detected through optical rectification and electro-optic sampling, respectively, in ZnTe crystals. Time-synchronized optical pulses at 800 nm were used as the pump for both the bulk Si and Si nanowire samples.

Figure 2a illustrates the electric-field waveform of the THz electromagnetic transient $E(t)$ transmitted through unexcited Si nanowires (solid line). Upon photoexcitation by the optical pump at 1.55 eV, a change in the transmitted THz waveform $\Delta E(t)$ is observed (dashed line). This example corresponds to a pump−probe delay time τ = 5 ps and pump fluence of 64 $\mu J/cm^2$. For all of the measurements, $\Delta E(t)$ is about 1−2% of $E(t)$ in magnitude and carries an opposite sign, corresponding to photoinduced absorption. As we discuss below, absorption of the pump photons leads to interband transitions in Si nanowires, and the density of photoexcited charge carriers at a given pump−probe delay time τ can be determined from a detailed Fourier analysis of the measured waveforms. The magnitude of the photoinduced change in the THz waveform at a fixed instance of time, for example, its peak t_0, $\Delta E(t_0)$, however, can be used to monitor the photoexcited carrier density approximately due to the slow variation of the spectral dependence of the photoinduced response.

In Figure 2b, we show the magnitude of $\Delta E(t_0;\tau)$ as a function of the pump−probe delay time τ (brown squares). The photoexcited carriers are seen to be present even ~0.7 ns after photoexcitation. The decay dynamics agrees well with an exponential function with a time constant of ~0.7 ns (solid line). The carrier lifetime varies with pump fluence, but not significantly. As a comparison, we also include in Figure 2b our result on bulk Si obtained using the same procedure. In this case, the photoinduced THz response remains mostly unchanged within the experimental time window. This result is consistent with the known long carrier lifetime (~μs) in pure Si single crystals due to the indirect gap nature of the material. Since the nanowires, fabricated from the bulk single crystal by chemical etching, retain the excellent bulk crystallinity, the substantially shortened carrier lifetime in nanowires is ascribed primarily to carrier trapping at the surfaces, which will be discussed in more detail below. The observed carrier lifetime in our Si nanowires, on the other hand, is several orders of magnitude longer than values reported in other Si nanostructures such as silicon nanocrystal films (~10 ps)[20] and microcrystalline silicon (μc-Si:H) (with a fast decay of ~0.7 ps).[25] The long lifetime of photoexcited carriers in our Si nanowires is advantageous for solar cell applications, and our result indicates that metal-assisted chemical etching is a preferred fabrication method for Si nanowires.

We now turn to a quantitative study of the transport properties of photoinduced charge carriers in Si nanowires by analyzing the spectral dependence of their responses. We use the thin film approximation to extract the photoinduced conductivity $\Delta\sigma(\omega)$ at frequency ω of the samples from the Fourier transform of the THz waveform transmitted through unexcited samples $E(\omega)$ and of its change upon photoexcitation $\Delta E(\omega)$:[26]

$$\Delta\sigma(\omega) = -\frac{\varepsilon_0 c(1+n_{sub})}{l}\times\frac{\Delta E(\omega)}{E(\omega)} \qquad (1)$$

Here, ε_0 is the permittivity of free space, c denotes the speed of light in vacuum, l is the sample thickness, and $n_{sub} = 1.96$ is the refractive index of the quartz substrate at the relevant THz frequencies. The thin film approximation is valid for samples of thickness much less than the THz wavelengths on transparent substrates as studied in this work. We have also assumed that the pump penetration depth far exceeds the film thickness, and the samples are uniformly excited.

Figure 3a,e illustrate the real and imaginary part of the complex conductivity spectrum extracted from the waveforms of Figure 2a. The conductivity spectrum cannot be described by the simple Drude model, which has successfully described the response of free charge carriers in bulk crystalline semiconductors including silicon.[27,28] The observed photoinduced conductivity is instead characteristic of a broad resonance: a peak in the real part of the conductivity, accompanied by a zero crossing in the imaginary part. We find that the

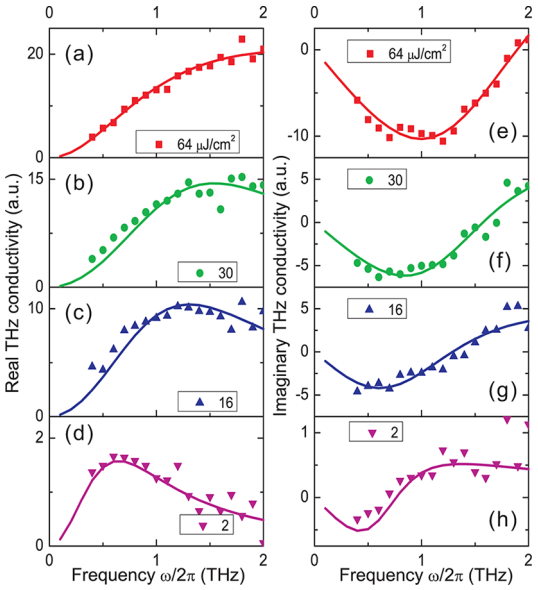

Figure 3. Pump fluence dependence of the THz photoconductivity at a fixed pump−probe delay τ = 5 ps. The real (a−d) and imaginary parts (e−h) of the photoinduced conductivity: (a) 2 μJ cm^{-2}, (b) 16 μJ cm^{-2}, (c) 30 μJ cm^{-2}, (d) 64 μJ cm^{-2}. Symbols are experimental data, and solid lines are fits to the Lorentz model, as described in the text.

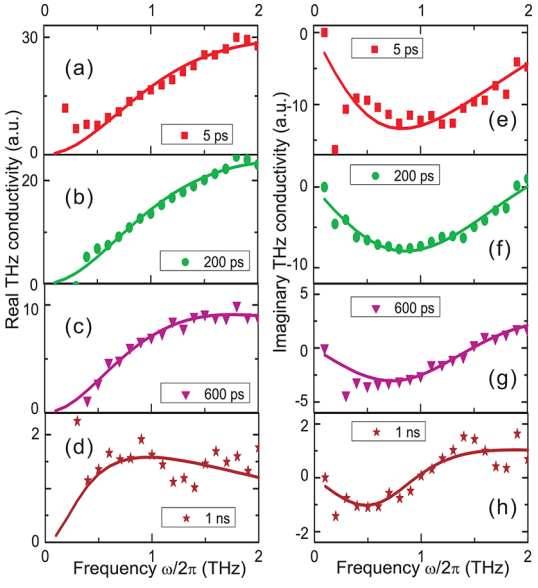

Figure 4. Dynamics of the photoinduced conductivity in Si nanowires for a fixed pump fluence of 64 μJ cm^{-2}. The real (a−d) and imaginary parts (e−h) of the photoinduced conductivity. Symbols are experimental data, and solid curves are fits to the Lorentz model.

spectrum can be described satisfactorily by the Lorentz model (solid lines)[19]

$$\delta(\omega) = \frac{\sigma_{sh}}{1 - i\omega\tau_D\left(1 - \frac{\omega_0^2}{\omega^2}\right)} \qquad (2)$$

where ω_0 and $1/\tau_D$ are the energy and width of the resonance, and σ_{sh} is the sheet conductivity at the peak of the resonance.

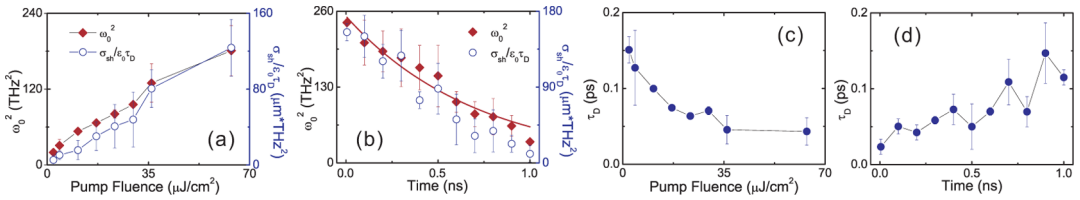

Figure 5. Parameters of the Lorentz model of eq 2 extracted from fits to the experimental THz conductivity spectra (symbols). Dependence on the pump fluence at a fixed pump−probe delay $\tau = 5$ ps (a,c) and dependence on the pump−probe delay time for a fixed pump fluence 64 μJ/cm^2 (b,d). Red line of (b) is an exponential dependence fit.

Similar measurements were performed for various pump fluences F and pump−probe delay times τ. Several representative photoinduced conductivity spectra are shown in Figure 3a−h for fluences ranging from 2 to 64 μJ cm^{-2} at a fixed delay of 5 ps and in Figure 4a−h for delay times ranging from 5 ps to 1 ns at a fixed pump fluence of 64 μJ cm^{-2}. We chose to probe carrier dynamics >5 ps after the photoexcitation to avoid the hot carrier effects. For all of the measurements, good agreement was obtained between the experimental spectra and the Lorentz model (solid lines) of eq 2. We summarize in Figure 5a,b the fitting parameters ω_0^2 and $\sigma_{sh}/\varepsilon_0\tau_D$ as a function of the pump fluence and delay time, respectively. Both ω_0^2 and $\sigma_{sh}/\varepsilon_0\tau_D$ increase approximately linearly with the pump fluence. These quantities decrease with increasing delay time, and the dependence can be described by an exponential function with a time constant of 710 and 680 ps, respectively. The time constants are comparable to the rough estimate obtained above by following the dynamics of the pump-induced change at the peak of the THz waveform.

What is the physical origin of the Lorentz resonances in the THz conductivity observed in photoexcited Si nanowires? The measured conductivity corresponds to the photoconductivity of the nanowire−air composites. To describe the linear response of the nanowire−air composite films with dilute, randomly distributed nanowires as in our case, an effective medium theory (EMT) such as the Maxwell−Garnett approximation[29,30] is often employed. It has been shown that for spherical particles with a Drude response and of diameters much smaller than the probe wavelengths the Maxwell−Garnett EMT leads to Lorentz resonances corresponding to surface plasmons.[31,32] The surface plasmon model has also been used to describe photoconductivity in nanowires and nanoparticles in refs 19, 33, and 34. Within this model, the parameters of eq 2 can be related to the density N and effective mass m_e^* of the free electron: $\sigma_{sh}/\varepsilon_0\tau_D = (Ne^2)/(\varepsilon_0 m_e^*)I$ and the surface plasmon resonance frequency $\omega_o^2 = (fNe^2)/(\varepsilon_\infty\varepsilon_0 m_e^*)$. Here $m_e^* = 0.26m_0$ denotes the electron effective mass, ε_∞ is the high-frequency dielectric response of Si, and f is a geometrical factor. In our case of long cylindrical nanowires lying on the substrate, $f = 1/2$ and 0 when the THz electromagnetic transient under normal incidence is polarized, respectively, perpendicular and parallel to the nanowire axis. Our observation of linear dependence of

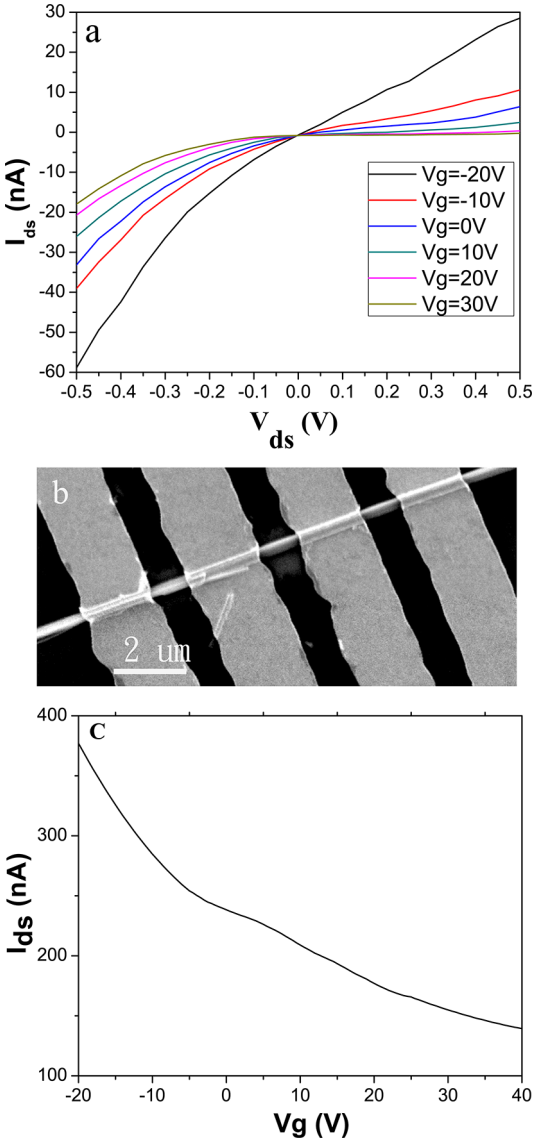

Figure 6. (a) $I_{ds}-V_{ds}$ characteristics of a single Si nanowire-based FET fabricated from an intrinsic Si wafer at gate voltage V_g varying from −20 to 30 V in steps of 10 V. (b) The SEM image of the device. (c) The transconductance curve of the nanowire.

$\sigma_{sh}/\varepsilon_0\tau_D$ and ω_o^2 on pump fluence is consistent with the model, and either quantity can be used to characterize the photoinduced carrier density. The photoinduced carrier density is extracted to be on the order of 10^{17} cm^{-3}, consistent with the estimate based on the absorbance of bulk Si. Our measurements also reveal the

carrier scattering time τ_D, a key transport parameter, for Si nanowires. Its dependence on the pump fluence and pump–probe delay time is illustrated in Figure 5c,d, respectively. The corresponding electron mobility can be estimated within the Drude framework, $\mu = e\tau_D/m_e^*$.[27] When the system is close to equilibrium (under low pump fluences and at long delay times), the extracted electron scattering time (0.15 ps) and mobility (1000 $cm^2/(V\cdot s)$) generally agree with that reported for bulk single-crystal Si.[24] The scattering time or mobility decreases at high pump fluences and at short delay times. A similar trend has also been observed in GaAs nanowires.[23] We note that both electron–electron and electron–phonon interactions would lead to a similar trend on the pump fluence and delay time. For the relatively low excitation densities as in our case, electron–electron scattering is negligible.

To further understand carrier scattering in Si nanowires, we performed transport studies on single-nanowire-based back-gated field-effect transistors in air at room temperature. A p-doped Si substrate is used as a global back gate. Figure 6 shows the output characteristics of a typical Si nanowire FET at various back-gate voltages (V_g), and Figure 6c shows the gate sweep characteristic at drain–source voltage V_{ds} = 1.5 V. It is characteristic of a p-type channel, common for Si NWs. The devices showed nearly linear gate dependence above the threshold. We used the transconductance in this linear region, $g_m = dI/dV_g$, to determine the mobility, μ, using the relation $g_m = \mu CV_{ds}/L^2$. Here, the channel length L = 1.2 μm and the capacitance $C = 1.51 \times 10^{-16}$ F. The electron mobility μ is determined to be 0.25 $cm^2/(V\cdot s)$. Using the measured mobility and resistivity, the carrier concentrations were evaluated with the Drude model to be about 10^{17} cm^{-3}, consistent with those reported by Jie *et al.*,[35] Luo *et al.*,[36] and Yuan *et al.*[17] Surfaces of our chemically etched Si NWs are known to be H-terminated after brief immersion in HF during the process. However, the hydrogen-terminated silicon surfaces are unstable and oxidize gradually upon exposure to ambient conditions. The H_2O and CO_2 in air adsorb on the silicon surfaces and are responsible for trapping electrons and rendering NWs p-doped. An accumulation layer is formed at the surface of Si nanowires as a result of surface band bending,[16,17] similar to that at diamond surfaces.[37] The drastic difference in the carrier mobility obtained from the THz and the dc transport measurement can be understood considering the nature of the two distinct measurements. In unexcited NWs, hole transport in the dc FET measurement is dominated by the surfaces and limited by surface defects. On the other hand, THz transport of photoexcited charge carriers (primarily of electrons due to their higher mobilities) is dominated by the inner region of the NWs.

CONCLUSIONS

In summary, we have studied the dynamics of photoexcited electrons in Si nanowires fabricated by chemical etching using the optical pump/THz probe spectroscopy. We have observed that the photoconductivity spectrum of Si nanowires is compatible with the surface plasmon model. By comparing to the surface plasmon model, we have obtained the electron density and scattering time in Si nanowires. We have found that the lifetime of photoexcited electrons is on the order of nanoseconds, and the carrier mobility in silicon nanowires is of similar magnitude as that in bulk silicon wafers. The diffusion length of electrons in nanowires at room temperature can be estimated from the diffusivity coefficient $D = {}^{\mu k_B T}/e$ and the carrier lifetime of t to be $(Dt)^{1/2} \sim 1.3$ μm. These properties are consequences of high crystallinity of the silicon nanowire arrays fabricated by metal-assisted wet chemical etching which involves no catalyst contamination. Combined with their excellent light-harvesting capabilities and the possibility of further surface modification to reduce surface defects,[1,18] these silicon nanowire arrays open new possibilities for PV applications.

EXPERIMENTAL SECTION

Synthesis of Si Nanowire Arrays. The precleaned Si wafers were immersed into a buffered oxide etchant for 2 min to remove the native oxide layer and then immediately transferred into a Ag deposition solution containing 4.8 M HF and 0.005 M $AgNO_3$ for 1 min at room temperature. The color of the Si surface changed from dark to colorful, indicating the formation of silver nanoparticles on the surface of silicon. The Ag-deposited silicon wafers were sufficiently rinsed with deionized water to remove extra silver ions and then immediately soaked into an etchant bath composed of 4.8 M HF and 0.3 M H_2O_2. The etching time was 1 h. Then the nanowire array was immersed in 15% HNO_3 solution for 1 min, washed by distilled water, followed by immersing in 2% HF for 3 min to etch the SiOx layer. This process was repeated three times to remove metal contamination on the surface.

Optical Pump/THz Probe Spectroscopy. A regenerative amplified Ti:sapphire laser system (Spectra Physics) producing 50 fs pulses centered at 800 nm (1.55 eV) and at 1 kHz repetition rate was used as the light source. Its output was split into three parts. One was used to induce conduction electrons in Si nanowires (with band gap of E_g = 1.12 eV), the other two to generate and detect THz electromagnetic transient through optical rectification and electro-optic sampling in two 1 mm thick ZnTe crystals, respectively. A combination of a lock-in amplifier and an optical chopper was employed for THz detection. For the detection of the transmitted THz pulse through an unexcited sample, the beam that generates the THz radiation was modulated, and for the detection of the pump-induced change in the THz radiation, the optical pump beam was modulated.

Measurement of Si Nanowire Field-Effect Transistor (FET). To investigate the electronic properties of the resulting nanowires etched from intrinsic silicon, we carried out electrical transport studies on individual nanowires using a simple back-gated FET device configuration on a silicon substrate. The underlying silicon was used as the back gate. To fabricate the device, silicon nanowires were deposited onto a SiO_2(300 nm)/Si substrate. Photolithography

followed by metal evaporation was used to define source and drain electrodes (Figure 6b). Electrical characterizations were carried out in ambient conditions at room temperature.

Conflict of Interest: The authors declare no competing financial interest.

Acknowledgment. This work was supported by the Research Grants Council of Hong Kong SAR, Grant No. CityU101909 at City University of Hong Kong, National Science Foundation under Grant No. DMR-0907477, and the Research Corporation Scialog Program at Case Western Reserve University.

REFERENCES AND NOTES

1. Shen, X. J.; Sun, B. Q.; Liu, D.; Lee, S. T. Hybrid Heterojunction Solar Cell Based on Organic−Inorganic Silicon Nanowire Array Architecture. *J. Am. Chem. Soc.* **2011**, *133*, 19408–19415.
2. Wang, X.; Peng, K. Q.; Pan, X. J.; Chen, X.; Li, Y. Y.; Meng, X. M.; Zhang, W. J.; Lee, S. T. High-Performance Silicon Nanowire Array Photoelectrochemical Solar Cells through Surface Passivation and Modification. *Angew. Chem., Int. Ed.* **2011**, *50*, 9861–9865.
3. Um, H. D.; Jung, J. Y.; Seo, H. S.; Park, K. T.; Jee, S. W.; Moiz, S. A.; Lee, J. H. Silicon Nanowire Array Solar Cell Prepared by Metal-Induced Electroless Etching with a Novel Processing Technology. *Jpn. J. Appl. Phys.* **2010**, *49*, 04DN02.
4. Kalita, G.; Adhikari, S.; Aryal, H. R.; Afre, R.; Soga, T.; Sharon, M.; Koichi, W.; Umeno, M. Silicon Nanowire Array/Polymer Hybrid Solar Cell Incorporating Carbon Nanotubes. *J. Phys. D: Appl. Phys.* **2009**, *42*, 115104.
5. Boettcher, S. W.; Spurgeon, J. M.; Putnam, M. C.; Warren, E. L.; Turner-Evans, D. B.; Kelzenberg, M. D.; Maiolo, J. R.; Atwater, H. A.; Lewis, N. S. Energy-Conversion Properties of Vapor−Liquid−Solid-Grown Silicon Wire-Array Photocathodes. *Science* **2010**, *327*, 185–187.
6. Kelzenberg, M. D.; Boettcher, S. W.; Petykiewicz, J. A.; Turner-Evans, D. B.; Putnam, M. C.; Warren, E. L.; Spurgeon, J. M.; Briggs, R. M.; Lewis, N. S.; Atwater, H. A. Enhanced Absorption and Carrier Collection in Si Wire Arrays for Photovoltaic Applications. *Nat. Mater.* **2010**, *9*, 239–244.
7. Tsakalakos, L.; Balch, J.; Fronheiser, J.; Korevaar, B. A.; Sulima, O.; Rand, J. Silicon Nanowire Solar Cells. *Appl. Phys. Lett.* **2007**, *91*, 233117.
8. Kelzenberg, M. D.; Putnam, M. C.; Turner-Evans, D. B.; Lewis, N. S.; Atwater, H. A. Predicted Efficiency of Si Wire Array Solar Cells. *34th IEEE Photovoltaic Specialists Conference PVSC* **2009**, 001948–001953.
9. Garnett, E.; Yang, P. D. Light Trapping in Silicon Nanowire Solar Cells. *Nano Lett.* **2010**, *10*, 1082–1087.
10. Hu, L.; Chen, G. Analysis of Optical Absorption in Silicon Nanowire Arrays for Photovoltaic Applications. *Nano. Lett* **2007**, *7*, 3249–3252.
11. Allen, J. E.; Hemesath, E. R.; Perea, D. E.; Lensch-Falk, J. L.; Li, Z. Y.; Yin, F.; Gass, M. H.; Wang, P.; Bleloch, A. L.; Palmer, R. E.; Lauhon, L. J. High-Resolution Detection of Au Catalyst Atoms in Si Nanowires. *Nat. Nanotechnol.* **2008**, *3*, 168–173.
12. Gunawan, O.; Guha, S. Characteristics of Vapor−Liquid−Solid Grown Silicon Nanowire Solar Cells. *Sol. Energy Mater. Sol. Cells* **2009**, *93*, 1388–1393.
13. Peng, K. Q.; Lu, A. J.; Zhang, R. Q.; Lee, S. T. Motility of Metal Nanoparticles in Silicon and Induced Anisotropic Silicon Etching. *Adv. Funct. Mater.* **2008**, *18*, 3026–3035.
14. Peng, K. Q.; Lee, S. T. Silicon Nanowires for Photovoltaic Solar Energy Conversion. *Adv. Mater.* **2011**, *23*, 198–215.
15. Kelzenberg, M. D.; Turner-Evans, D. B.; Kayes, B. M.; Filler, M. A.; Putnam, M. C.; Lewis, N. S.; Atwater, H. A. Photovoltaic Measurements in Single-Nanowire Silicon Solar Cells. *Nano. Lett* **2008**, *8*, 710–714.
16. Guo, C. S.; Luo, L. B.; Yuan, G. D.; Yang, X. B.; Zhang, R. Q.; Zhang, W. J.; Lee, S. T. Surface Passivation and Transfer Doping of Silicon Nanowires. *Angew. Chem., Int. Ed.* **2009**, *48*, 9896–9900.
17. Yuan, G. D.; Zhou, Y. B.; Guo, C. S.; Zhang, W. J.; Tang, Y. B.; Li, Y. Q.; Chen, Z. H.; He, Z. B.; Zhang, X. J.; Wang, P. F.; Bello, I.; Zhang, R. Q.; Lee, C. S.; Lee, S. T. Tunable Electrical Properties of Silicon Nanowires *via* Surface-Ambient Chemistry. *ACS Nano* **2010**, *4*, 3045–3052.
18. Zhang, F. T.; Sun, B. Q.; Song, T.; Zhu, X. L.; Lee, S. T. Air Stable, Efficient Hybrid Photovoltaic Devices Based on Poly(3-hexylthiophene) and Silicon Nanostructures. *Chem. Mater.* **2011**, *23*, 2084–2090.
19. Ulbricht, R.; Hendry, E.; Shan, J.; Heinz, T. F. Carrier Dynamics in Semiconductors Studied with Time-Resolved Terahertz Spectroscopy. *Rev. Mod. Phys.* **2011**, *83*, 543–586.
20. Cooke, D. G.; MacDonald, A. N.; Hryciw, A.; Wang, J.; Li, Q.; Meldrum, A.; Hegmann, F. A. Transient Terahertz Conductivity in Photoexcited Silicon Nanocrystal Films. *Phys. Rev. B* **2006**, *73*, 193311.
21. Wang, F.; Shan, J.; Bonn, M.; Islam, M.; Herman, I.; Heinz, T. F. Exciton Polarizability in Semiconductor Nanocrystals. *Nat. Mater.* **2006**, *5*, 861–864.
22. Richter, C.; Schmuttenmaer, C. A. Exciton-like Trap States Limit Electron Mobility in TiO_2 Nanotubes. *Nat. Nanotechnol.* **2010**, *5*, 769–772.
23. Parkinson, P.; Lloyd-Hughes, J.; Gao, Q.; Tan, H. H.; Jagadish, C.; Johnston, M. B.; Herz, L. M. Transient Terahertz Conductivity of GaAs Nanowires. *Nano Lett.* **2007**, *7*, 2162–2165.
24. Strait, J. H.; George, P. A.; Levendorf, M.; Blood-Forsythe, M.; Rana, A.; Park, J. Measurements of the Carrier Dynamics and Terahertz Response of Oriented Germanium Nanowires Using Optical-Pump Terahertz-Probe Spectroscopy. *Nano Lett.* **2009**, *9*, 2967–2972.
25. Jepsen, P. U.; Schairer, W.; Libon, I. H.; Lemmer, U.; Hecker, N. E.; Birkholz, M.; Lips, K.; Schall, M. Ultrafast Carrier Trapping in Microcrystalline Silicon Observed in Optical Pump - Terahertz Probe Measurements. *Appl. Phys. Lett.* **2001**, *79*, 1291–1293.
26. Kuzel, P.; Kadlec, F.; Nemec, H. Propagation of Terahertz Pulses in Photoexcited Media: Analytical Theory for Layered Systems. *J. Chem. Phys.* **2007**, *127*, 024506.
27. Jeon, T. I.; Grischkowsky, D. Nature of Conduction in Doped Silicon. *Phys. Rev. Lett.* **1997**, *78*, 1106–1109.
28. Beard, M. C.; Turner, G. M.; Schmuttenmaer, C. A. Transient Photoconductivity in GaAs as Measured by Time-Resolved Terahertz Spectroscopy. *Phys. Rev. B* **2000**, *62*, 15764–15777.
29. Garnett, J. C. M. Colours in Metal Glasses and in Metallic Films. *Philos. Trans. R. Soc., A* **1904**, *203*, 385–420.
30. Bruggemann, D. A. G. Berechnung verschiedener physikalischer Konstanten von heterogenen Substanzen. A. *Ann. Phys. (Leipzig)* **1935**, *24*, 636–679.
31. Spanier, J. E.; Herman, I. P. Use of Hybrid Phenomenological and Statistical Effective-Medium Theories of Dielectric Functions to Model the Infrared Reflectance of Porous SiC Films. *Phys. Rev. B* **2000**, *61*, 10437–10450.
32. Kirchner, A.; Busch, K.; Soukoulis, C. M. Transport Properties of Random Arrays of Dielectric Cylinders. *Phys. Rev. B* **1998**, *57*, 277–288.
33. Nienhuys, H. K.; Sundstrom, V. Influence of Plasmons on Terahertz Conductivity Measurements. *Appl. Phys. Lett.* **2005**, *87*, 012101.
34. Zayats, A. V.; Smolyaninov, I. I. Near-Field Photonics: Surface Plasmon Polaritons and Localised Surface Plasmons. *J. Opt. A: Pure Appl. Opt.* **2003**, *5*, S16–S50.
35. Jie, J. S.; Zhang, W. J.; Peng, K. Q.; Yuan, G. D.; Lee, C. S.; Lee, S. T. The Surface-Dominated Transport Properties of Silicon Nanowires. *Adv. Funct. Mater.* **2008**, *18*, 3251–3257.
36. Luo, L. B.; Yang, X. B.; Liang, F. X.; Xu, H.; Zhao, Y.; Xie, X.; Zhang, W. F.; Lee, S. T. Surface Defects-Induced p-Type Conduction of Silicon Nanowires. *J. Phys. Chem. C* **2011**, *115*, 18453–18458.
37. Maier, F.; Riedel, M.; Mantel, B.; Ristein, J.; Ley, L. Origin of Surface Conductivity in Diamond. *Phys. Rev. Lett.* **2000**, *85*, 3472–3475.